

Position Control of an Over-Actuated Direct Hydraulic Cylinder Drive

Lasse Schmidt^a, Morten Groenkjaer^a, Henrik C. Pedersen^a, Torben O. Andersen^a

^a*Department of Energy Technology, Aalborg University, Denmark*

Abstract

This paper considers the analysis and control strategy for a novel direct hydraulic cylinder drive, that is over-actuated in the sense that it has more inputs than sensible outputs. Efforts to overcome the inherent loss of energy due to throttling in valve driven hydraulic drives are many, and various approaches have been proposed by research communities as well as the industry. Recently, a so-called Speed-variable Switched Differential Pump was proposed for direct drive of hydraulic differential cylinders. The main idea with this drive is to utilize an electric rotary drive with the shaft connected to three oppositely oriented fixed displacement gear pumps to actuate a differential cylinder. To ensure a high stiffness of the drive, this is constructed such that the transmission line pressures will increase for pump output flows exceeding pump leakages, and proportional valves provides the ability to bleed off flow from the transmission lines to achieve reasonable pressure levels. This design renders the drive over-actuated as the line pressures and the cylinder piston motion cannot be controlled independently, due to the pressure difference being motion generating. In order to achieve satisfactory performance of this drive, a state coupling analysis is presented along with a control strategy based on state decoupling synthesized from input-output transformations. This includes control schemes for the transformed system. The proposed control strategy is experimentally verified on a drive prototype, and results demonstrate that satisfactory overall performance-, and in particular highly accurate position tracking is achieved.

Keywords: Electro-Hydraulic Drives, Direct Hydraulic Drives, Motion Control, Pressure Control, Over Actuated Systems, Input-Output Transformation

1. Introduction

Linear hydraulic drives realized with cylinders are widely used in industry due to well known advantages such as their high power- and force densities and possibly fast and accurate responses, and here particularly differential cylinders are used. Actuation of hydraulic cylinders is conventionally established by use of proportional valves, supplied by variable displacement pumps operated at constant shaft speeds, often targeting a constant pressure level. As the valve flows are generated by throttling over the valve ports, this may be associated with significant power losses. The reduction of losses may be achieved while maintaining valve actuation by different methods, e.g. by controlling the pump outlet pressure (valve supply pressure) actively, or by utilization of an additional proportional valve such that so-called separate-meter-in-separate-meter-out operation can be established.

Other approaches to actuate hydraulic cylinders include the elimination of the throttle driven main flow. In recent years various approaches have been presented by research communities and the industry. The main focus has been on proportional flow control devices based on variable displacement units, rectifying bridges and/or accumulator solutions, rendering these solutions rather complex and/or costly, see e.g. [1, 2, 3]. Another relevant approach to reduce throttle losses is the use of digital hydraulics. In e.g. [4] digital hydraulic displacement technology was used for differential hydraulic cylinder operation, and in [5] a digital displacement pump was considered for a hydraulic wind turbine transmission, which also has perspectives in regard to differential cylinder actuation.

Also, attention has been given to speed-variable solutions based on fixed displacement pumps for use in speed-, pressure- and flow control applications [6], and for differential cylinder operation [7, 8]. A review on the topic of direct hydraulic cylinder drives is considered in [9]. Recently, a so-called *Speed-variable Switched Differential Pump* (SvSDP) was presented in [10], which

*Corresponding author

Email address: 1sc@et.aau.dk (Lasse Schmidt)

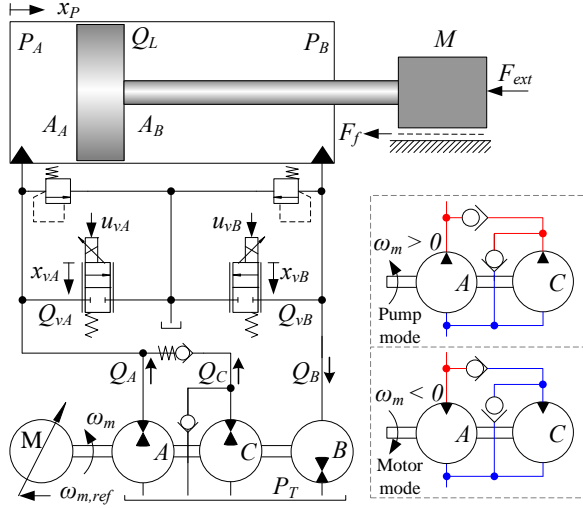


Figure 1: Cylinder actuated by Speed-variable Switched Differential Pump (SvSDP) drive.

is a modified version of the SvDP drive presented in [8]. The SvSDP design utilizes three fixed displacement pumps and targets proper dynamic properties and a high energy efficiency due to reduced throttling losses. The SvSDP drive concept is depicted in figure 1. The SvSDP is designed based on the idea that the return chamber pressure *ideally* always should increase, and *realistically* this is the case only above some lower shaft speed, due to leakage in the pumps. With cross port leakage absent, i.e. $Q_L = 0$, this is realized when the pump output flows satisfy (1) or (2).

$$\alpha(Q_A + Q_C) > Q_B \text{ for } \omega_m > 0 \quad (1)$$

$$\alpha Q_A < Q_B \text{ for } \omega_m < 0 \quad (2)$$

Indeed, with (1) or (2) satisfied, pressures will build up continuously until one of the pressures reaches the opening pressure of the relief valves, and otherwise *at least* one of the pressures will tend to the reservoir pressure [8]. Hence for e.g. a constant load force, the pressures will only remain constant provided that $\alpha(Q_A + Q_C) = Q_B$ for $\omega_m > 0$ or $\alpha Q_A = Q_B$ for $\omega_m < 0$. Therefore, in order to achieve a proper drive performance, 2/2 proportional valves are installed, enabling the possibility to bleed off excess compression flow, when (1) or (2) are satisfied. However, the chamber pressures cannot be controlled independently without influencing the cylinder output force, and hence the piston motion. Therefore, it is only reasonable to control the piston motion and one of the chamber pressures, rendering the drive over-actuated in the sense that there are three inputs and only two sensible outputs. Hence,

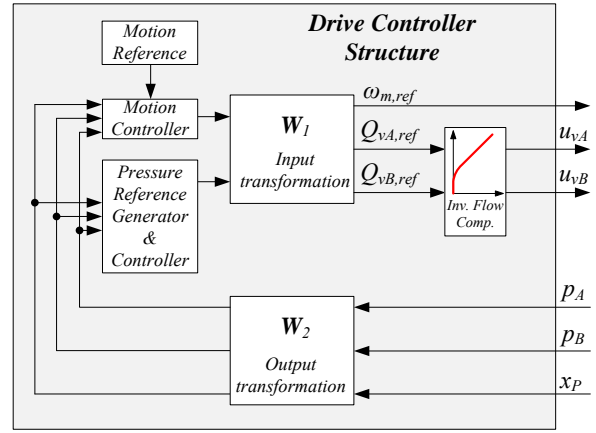


Figure 2: Main structure of proposed control scheme.

in order for the drive to be operated properly, some appropriate control strategy must be considered.

The control of over-actuated systems and the problem of allocation/distribution of input signals in such systems has been considered in various literature. For example this was considered in relation to a quad-rotor aerial vehicle in [11], to e.g. ground vehicles in [12, 13] and when combined with fault tolerant control in [14], to name a few. In relation to fault tolerant control, this was also considered in [15] when combined with sliding mode control. A survey on the topic of control allocation was recently published in [16]. Research literature related to control of- and control allocation in over-actuated hydraulic systems appear to be limited, however this is considered in [17] in relation to networked hydraulic systems.

This paper presents an approach to handle the problem of allocation/distribution of inputs for the SvSDP drive based on input-output transformation, which to some extend resembles those of field oriented controllers for electric machines, and is depicted in figure 2. The input-output transformation proposed is based on physical reasoning, using only measurements of the piston position and transmission line pressures as feedback. This transformation allows to decouple the motion control from the chamber pressure control, such that the piston motion can be controlled independently of the chamber pressures. After modeling of the drive, a coupling analysis is presented based on the relative gain arrays, and from this, an output transformation based on some auxiliary virtual pressure state is established. A corresponding input transformation allows to generate references for the transformed output states, and combined with additional piston position- and pressure controllers, a linear parameter varying control scheme

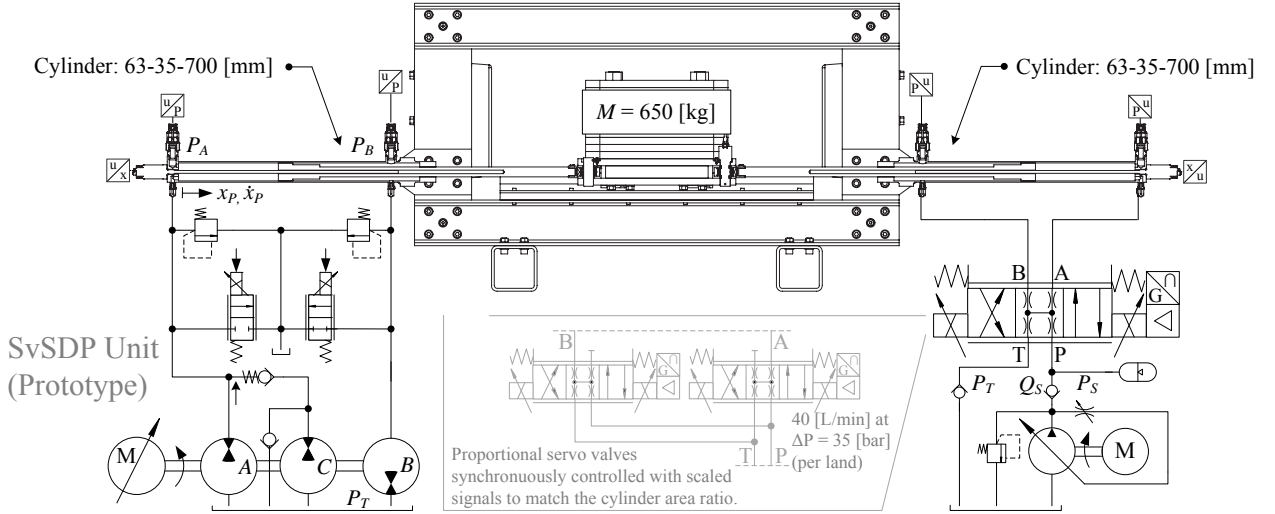


Figure 3: Test bench with SvSDP prototype drive (Aalborg University, Denmark).

is synthesized, demonstrating a nearly complete decoupling of the system states. The performance of the proposed control strategy is verified through experimental results.

2. Model of SvSDP Actuated Cylinder Drive

Utilizing the notation in figure 1 and defining $V_A = V_{A0} + A_A x_P$, $V_B = V_{B0} - A_B x_P$, $\alpha = A_B/A_A$, and noting state dependencies $\eta_{vA} = \eta_{vA}(\omega_m, P_A)$, $\eta_{vB} = \eta_{vB}(\omega_m, P_B)$, $\eta_{vC} = \eta_{vC}(\omega_m, P_A)$, the system may be described by Eqs. (3)–(11), assuming cross-port leakage Q_L negligible.

$$\ddot{x}_P = M^{-1}(A_A(P_A - \alpha P_B) - B_v \dot{x}_P - F_f - F_{ext}) \quad (3)$$

$$\dot{P}_A = \frac{\beta_{Ae}}{V_A}(Q_A - Q_{vA} - A_A \dot{x}_P) \quad (4)$$

$$\dot{P}_B = \frac{\beta_{Be}}{V_B}(\alpha A_A \dot{x}_P - Q_B - Q_{vB}) \quad (5)$$

$$Q_A = \begin{cases} \bar{Q}_A(\omega_m)\eta_{vA} + \bar{Q}_C(\omega_m)\eta_{vC} & \text{for } \omega_m \geq 0 \\ \bar{Q}_A(\omega_m)/\eta_{vA} & \text{for } \omega_m < 0 \end{cases} \quad (6)$$

$$Q_B = \begin{cases} \bar{Q}_B(\omega_m)/\eta_{vB} & \text{for } \omega_m \geq 0 \\ \bar{Q}_B(\omega_m)\eta_{vB} & \text{for } \omega_m < 0 \end{cases} \quad (7)$$

$$Q_{vA} = K_{vA}(x_{vA})x_{vA}, \quad Q_{vB} = K_{vB}(x_{vB})x_{vB} \quad (8)$$

$$\ddot{x}_{vA} = \omega_{vA}^2 u_{vA} - 2\zeta_{vA}\omega_{vA} \dot{x}_{vA} - \omega_{vA}^2 x_{vA} \quad (9)$$

$$\ddot{x}_{vB} = \omega_{vB}^2 u_{vB} - 2\zeta_{vB}\omega_{vB} \dot{x}_{vB} - \omega_{vB}^2 x_{vB} \quad (10)$$

$$\ddot{\omega}_m = \omega_v^2 \omega_{m,ref} - 2\zeta_v \omega_v \dot{\omega}_m - \omega_v^2 \omega_m \quad (11)$$

Here \bar{Q}_A , \bar{Q}_B and \bar{Q}_C are theoretical pump flows, P_A and P_B chamber pressures, ω_m the motor shaft speed,

x_P the cylinder piston position and x_{vA} , x_{vB} the valve spool positions. The inputs are the motor shaft reference speed $\omega_{m,ref}$ and the valve inputs u_{vA} , u_{vB} . Furthermore, B_v is a viscous friction coefficient, F_f nonlinear friction forces, V_{A0} , V_{B0} initial volumes, ζ_{vA} , ζ_{vB} , ζ_v damping ratios, ω_{vA} , ω_{vB} , ω_v bandwidths, β_{Ae} , β_{Be} the effective bulk moduli and $K_{vA} = K_{vA}(x_{vA})$, $K_{vB} = K_{vB}(x_{vB})$ are the flow gains of the 2/2 valves. Note that the 2/2 proportional valves are pressure compensated and produces output flows that are nearly proportional to the valve spool displacements beyond spool overlaps.

2.1. SvSDP Prototype Testbench

The following sections take offset in the SvSDP prototype drive installed in a physical test bench placed at Aalborg University, Aalborg, Denmark, shown in figure 3. The communication setup in the test bench is sketched in figure 4, and the main components of the SvSDP prototype drive are outlined in table 1.

As depicted in figure 3 the test bench consists of two opposing, identical cylinders, driven by the SvSDP prototype (main cylinder) and by a conventional valve setup (load cylinder), respectively.

3. Linear Model & State Coupling Analysis

The 2/2 valves are pressure compensated why the inverse flow characteristics is be used to compensate the input such that in the ideal case $Q_{vA} = Q_{vA,ref}$, $Q_{vB} = Q_{vB,ref}$, while assuming the valve dynamics negligible.

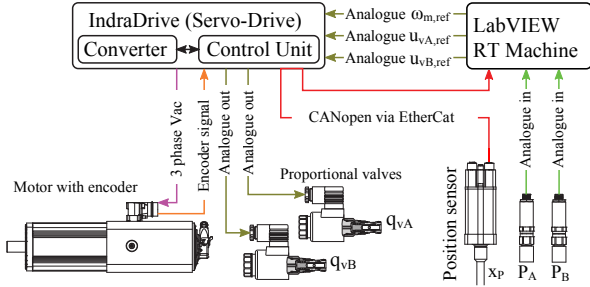


Figure 4: Test bench communication setup (Aalborg University, Denmark).

Component	Description
^a IndraDyn S-MSK071E	Servo motor
^a IndraDrive HCS02.1E	Converter
^a CSH01.1C-ET-ENS	Control unit
^a AZPFFF-12-016/014/011	Pump rack
^a KKDSR1NB	2/2 prop. valves
^a HM 17-1X/250	Pres. sensor(s)
^b Cylinder 63-35-700	Hyd. cylinder
^c BTL7-V50E (EtherCAT)	Position sensor
^d LabVIEW RT Desktop with NI-DAQmx	Control system

Table 1: Main components of SvSDP prototype drive. ^aBosch Rexroth AG, ^bFjero A/S, ^cBalluf GmbH, ^dNational Instruments Corporation.

3.1. Linear Plant Model

Omitting the motor- and valve dynamics, the pump flows depend on the volumetric efficiencies that are dependent on the pump pressure differences and the shaft speed. The linear model equations are established assuming constant effective bulk moduli and are given by Eqs. (12)–(16) where external forces and nonlinear friction characteristics are omitted, defining the relations $\rho = V_B/V_A$, $\rho_0 = V_{0B}/V_{0A}$ with $V_{0A} = V_A|_{\mathbf{x}_0}$, $V_{0B} = V_B|_{\mathbf{x}_0}$ and \mathbf{x}_0 being the state vector at the linearization point where p denote pressure deviation variables.

$$\ddot{x}_P = M^{-1}(A_A(p_A - \alpha p_B) - B_v \dot{x}_P) \quad (12)$$

$$\dot{p}_A = \frac{\beta_e}{V_{0A}}(K_{Aq}\omega_m - K_{Aqp}p_A - q_{vA} - A_A \dot{x}_P) \quad (13)$$

$$\dot{p}_B = \frac{\beta_e}{\rho_0 V_{0A}}(\alpha A_A \dot{x}_P - K_{Bq}\omega_m + K_{Bqp}p_B - q_{vB}) \quad (14)$$

$$K_{Aq} = \left. \frac{\partial Q_A}{\partial \omega_m} \right|_{\mathbf{x}_0}, \quad K_{Bq} = \left. \frac{\partial Q_B}{\partial \omega_m} \right|_{\mathbf{x}_0} \quad (15)$$

$$K_{Aqp} = \left. \frac{\partial Q_A}{\partial P_A} \right|_{\mathbf{x}_0}, \quad K_{Bqp} = \left. \frac{\partial Q_B}{\partial P_B} \right|_{\mathbf{x}_0} \quad (16)$$

The linear model equations for the plant without actuator dynamics may be represented in a state space form as:

$$\dot{\mathbf{x}}_p = \mathbf{A}_p \mathbf{x}_p + \mathbf{B}_p \mathbf{u}_p, \quad \mathbf{y}_p = \mathbf{C}_p \mathbf{x}_p \quad (17)$$

$$\mathbf{x}_p = [x_P \dot{x}_P p_A p_B]^T, \quad \mathbf{u}_p = [\omega_m q_{vA} q_{vB}]^T$$

$$\mathbf{y}_p = [x_P p_A p_B]^T, \quad \mathbf{C}_p = \begin{bmatrix} 1 & 0 & 0 & 0 \\ 0 & 0 & 1 & 0 \\ 0 & 0 & 0 & 1 \end{bmatrix}$$

$$\mathbf{A}_p = \begin{bmatrix} 0 & 1 & 0 & 0 \\ 0 & -\frac{B_v}{M} & \frac{A_A}{M} & -\frac{\alpha A_A}{M} \\ 0 & -\frac{\beta_e A_A}{V_{0A}} & -\frac{\beta_e K_{Aqp}}{V_{0A}} & 0 \\ 0 & \frac{\beta_e \alpha A_A}{\rho_0 V_{0A}} & 0 & \frac{\beta_e K_{Bqp}}{\rho_0 V_{0A}} \end{bmatrix}$$

It is notable that ρ_0 is a function of the linearization point as this is a function of the system state. This fact will be used in later sections for update of the control proposed control structure.

The linear model (17) may be expressed by the transfer function (18) with s being the Laplace frequency.

$$\mathbf{y}_p(s) = \mathbf{G}_p(s)\mathbf{u}_p(s), \quad \mathbf{G}_p(s) = \mathbf{C}_p(s\mathbf{I} - \mathbf{A}_p)^{-1}\mathbf{B}_p \quad (18)$$

3.2. Linear Actuator Model

The linear model for the actuator dynamics is given by:

$$\dot{\mathbf{x}}_u = \mathbf{A}_u \mathbf{x}_u + \mathbf{B}_u \mathbf{u}_u, \quad \mathbf{y}_u = \mathbf{C}_u \mathbf{x}_u, \quad (19)$$

$$\mathbf{y}_u = \mathbf{u}_p = [\omega_m q_{vA} q_{vB}]^T, \quad \mathbf{u}_{ref} = [\omega_{m,ref} q_{vA,ref} q_{vB,ref}]^T$$

$$\mathbf{x}_u = [\omega_m \dot{\omega}_m q_{vA} \dot{q}_{vA} q_{vB} \dot{q}_{vB}]^T$$

$$\mathbf{A}_u = \begin{bmatrix} \mathbf{A}_{u1} & \mathbf{0} & \mathbf{0} \\ \mathbf{0} & \mathbf{A}_{u2} & \mathbf{0} \\ \mathbf{0} & \mathbf{0} & \mathbf{A}_{u3} \end{bmatrix}, \quad \mathbf{A}_{u1} = \begin{bmatrix} 0 & 1 \\ -\omega_v^2 & -2\zeta_v \omega_v \end{bmatrix}$$

$$\mathbf{A}_{u2} = \begin{bmatrix} 0 & 1 \\ -\omega_{vA}^2 & -2\zeta_{vA} \omega_{vA} \end{bmatrix}, \quad \mathbf{A}_{u3} = \begin{bmatrix} 0 & 1 \\ -\omega_{vB}^2 & -2\zeta_{vB} \omega_{vB} \end{bmatrix}$$

$$\mathbf{B}_u = \begin{bmatrix} 0 & 0 & 0 \\ \omega_v^2 & 0 & 0 \\ 0 & 0 & 0 \\ 0 & \omega_{vA}^2 & 0 \\ 0 & 0 & 0 \\ 0 & 0 & \omega_{vB}^2 \end{bmatrix}, \quad \mathbf{C}_u = \begin{bmatrix} 1 & 0 & 0 & 0 & 0 & 0 \\ 0 & 0 & 1 & 0 & 0 & 0 \\ 0 & 0 & 0 & 0 & 1 & 0 \end{bmatrix}$$

Similar to the plant model, the actuator model (19) may be expressed by the transfer function (20).

$$\mathbf{y}_u(s) = \mathbf{G}_u(s)\mathbf{u}_{ref}(s), \mathbf{G}_u(s) = \mathbf{C}_u(s\mathbf{I} - \mathbf{A}_u)^{-1}\mathbf{B}_u \quad (20)$$

3.3. Extended Linear Model

The combined input-output linear model, denoted the *extended* linear model, is given by:

$$\begin{aligned} \dot{\mathbf{x}}_e &= \mathbf{A}_e \mathbf{x}_e + \mathbf{B}_e \mathbf{u}_{ref}, \quad \mathbf{y} = \mathbf{C}_e \mathbf{x}_e \quad (21) \\ \mathbf{x}_e &= \begin{bmatrix} \mathbf{x}_p \\ \mathbf{x}_u \end{bmatrix}, \quad \mathbf{A}_e = \begin{bmatrix} \mathbf{A}_p & \mathbf{B}_p \mathbf{C}_u \\ \mathbf{0} & \mathbf{A}_u \end{bmatrix} \\ \mathbf{B}_e &= \begin{bmatrix} \mathbf{0} \\ \mathbf{B}_u \end{bmatrix}, \quad \mathbf{C}_e = \begin{bmatrix} \mathbf{C}_p & \mathbf{0} \end{bmatrix} \end{aligned}$$

Written in a transfer function matrix form, the model (21) is given by:

$$\mathbf{y}_p(s) = \mathbf{G}_e(s)\mathbf{u}_{ref}(s), \quad \mathbf{G}_e(s) = \mathbf{C}_e(s\mathbf{I} - \mathbf{A}_e)^{-1}\mathbf{B}_e \quad (22)$$

3.4. Coupling Analysis

In order to evaluate the strength of the couplings between the inputs and outputs and assign these some measure, a relative gain array (RGA) analysis is utilized. In the specific case considered, the outputs are the piston position and chamber pressures. It is not possible to control both chamber pressures and the piston position independently, and therefore the cross-couplings of the system are considered for all sensible combinations. To investigate the reasonable input-output combinations, the system (22) is divided into smaller subsystems with $\mathbf{G}_k(s) = \mathbf{G}_k$, $k = 1..6$ being 2×2 sub matrices of $\mathbf{G}_e(s)$. These are given by:

$$\begin{aligned} \mathbf{G}_1 &= \begin{bmatrix} g_{11} & g_{12} \\ g_{21} & g_{22} \end{bmatrix}, \quad \mathbf{G}_2 = \begin{bmatrix} g_{11} & g_{13} \\ g_{21} & g_{23} \end{bmatrix}, \quad \mathbf{G}_3 = \begin{bmatrix} g_{11} & g_{12} \\ g_{31} & g_{32} \end{bmatrix} \\ \mathbf{G}_4 &= \begin{bmatrix} g_{11} & g_{13} \\ g_{31} & g_{33} \end{bmatrix}, \quad \mathbf{G}_5 = \begin{bmatrix} g_{21} & g_{22} \\ g_{31} & g_{32} \end{bmatrix}, \quad \mathbf{G}_6 = \begin{bmatrix} g_{21} & g_{23} \\ g_{31} & g_{33} \end{bmatrix} \end{aligned}$$

The relative gain array number RGAn defined as Eq. (23) for diagonal pairings and Eq. (24) for off-diagonal pairings, where $.*$ denotes the Schur product, is utilized to visualize the properties of the system couplings:

$$\text{RGAn}_d(\omega) = \|\mathbf{H}\|_\Sigma = \sum_{i,j} |h_{i,j}| \quad (23)$$

$$\text{RGAn}_{od}(\omega) = \|\check{\mathbf{H}}\|_\Sigma = \sum_{i,j} |\check{h}_{i,j}| \quad (24)$$

$$\mathbf{H} = \mathbf{G}_k(j\omega) .* (\mathbf{G}_k^{-1}(j\omega))^T - \begin{bmatrix} 1 & 0 \\ 0 & 1 \end{bmatrix}, \quad k = 1..6 \quad (25)$$

$$\check{\mathbf{H}} = \mathbf{G}_k(j\omega) .* (\mathbf{G}_k^{-1}(j\omega))^T - \begin{bmatrix} 0 & 1 \\ 1 & 0 \end{bmatrix}, \quad k = 1..6 \quad (26)$$

In the event of an ideal decoupling of the system, then $\text{RGAn}_d = 0$ and $\text{RGAn}_{od} = 4$ for all possible frequencies.

The RGA number for the diagonal and off-diagonal elements of the transfer function sub-matrices are shown in figure 5. It is found that all pairings exhibits similar behavior near what is the system eigenfrequency. Here the RGA numbers tend to increase highly above the desired values of 0 and 4 for diagonal- and off-diagonal pairings, respectively, implying that decentralized control may only be implemented successfully, when the closed loop bandwidths are comfortably below the system eigenfrequency. In particular, figures 5 (a)-(d) imply that the piston position should be controlled by the electrical servo drive, whereas either of the chamber pressures can be controlled by the proportional valves.

From the above analysis, decentralized control should not be applied directly due to the strong dynamic couplings. In addition, from figure 5, the *proper* pairings changes for frequencies above the system eigenfrequency. A strategy could be to accept the cross-couplings, and use e.g. an LQR approach to establish an overall system controller. However, it is not trivial to include the single-directional valve flow constraint and furthermore such an approach necessitates full state feedback, often not available in e.g. hydraulic cylinder drives operating under industrial conditions.

An alternative strategy is to decouple the motion and chamber pressure dynamics in order to simplify the design process, and such that the controller designs may be separated from the valve signal allocation approach. This was attempted in a special case in [10], based on the physical couplings in the system. In the following, this concept is generalized.

4. Input-Output Transformation

Basically, the idea is to decouple the system states in some proper way utilizing the transformation matrices \mathbf{W}_1 , \mathbf{W}_2 , such that input- and output variables are changed according to $\tilde{\mathbf{y}} = \mathbf{W}_2 \mathbf{y}_p$, $\tilde{\mathbf{u}} = \mathbf{W}_1^{-1} \mathbf{u}_{ref}$. Consider Eqs. (27), (28), omitting the Laplace notion (s) for brevity.

$$\mathbf{u}_p = \mathbf{G}_u \mathbf{u}_{ref}, \quad \mathbf{u}_{ref} = \mathbf{W}_1 \tilde{\mathbf{u}} \Rightarrow \mathbf{u}_p = \mathbf{G}_u \mathbf{W}_1 \tilde{\mathbf{u}} \quad (27)$$

$$\tilde{\mathbf{y}} = \mathbf{W}_2 \mathbf{y}_p, \quad \mathbf{y}_p = \mathbf{G}_p \mathbf{u}_p \Rightarrow \tilde{\mathbf{y}} = \mathbf{W}_2 \mathbf{G}_p \mathbf{u}_p \quad (28)$$

Combining Eqs. (27), (28), the transformed system is obtained as:

$$\tilde{\mathbf{y}} = \tilde{\mathbf{G}}_e \tilde{\mathbf{u}}, \quad \tilde{\mathbf{G}}_e = \mathbf{W}_2 \mathbf{G}_p \mathbf{G}_u \mathbf{W}_1 = \mathbf{W}_2 \mathbf{G}_e \mathbf{W}_1 \quad (29)$$

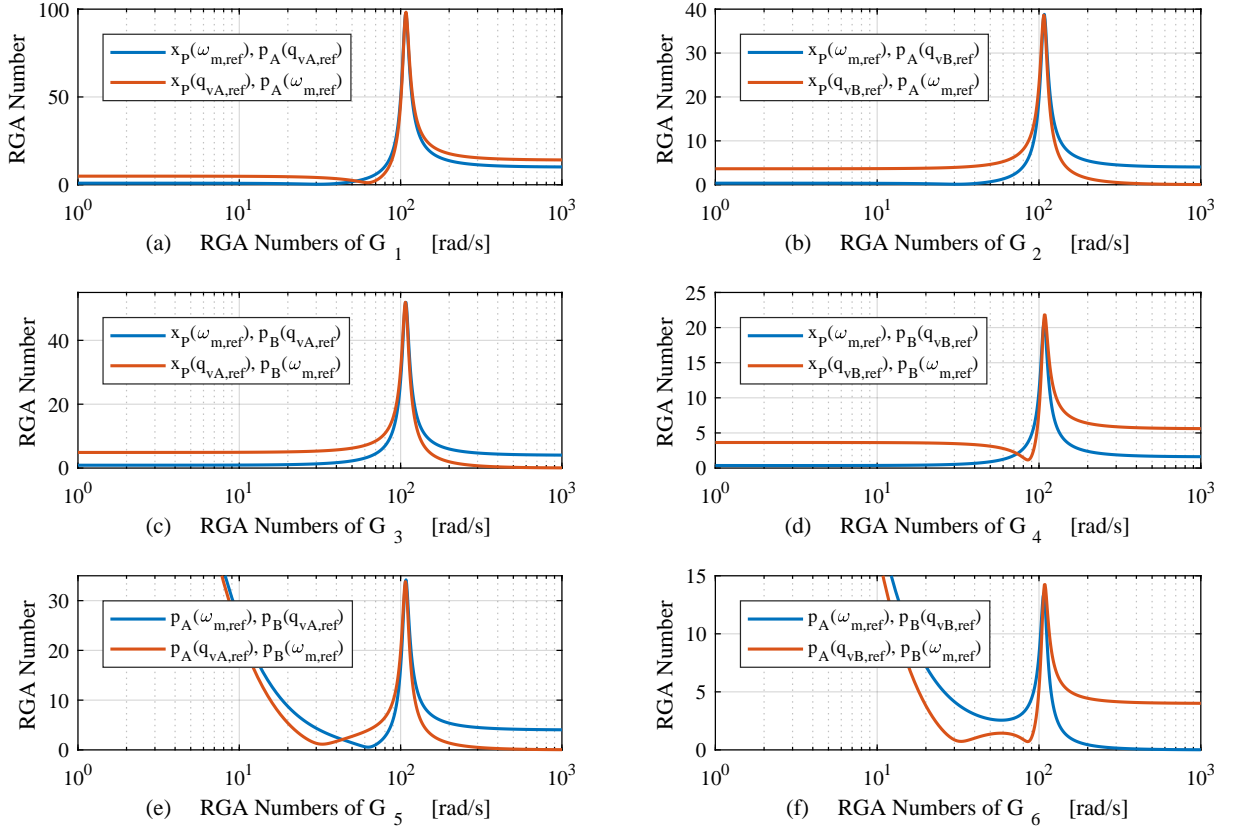


Figure 5: RGA numbers for diagonal- and off-diagonal pairings for different input-output combinations.

165 As the static gain of $\mathbf{G}_u(s)$ is unity, i.e. $\mathbf{G}_u(0) = \mathbf{I}$, the static transformation matrices $\mathbf{W}_1, \mathbf{W}_2$ may be designed from the plant model (18).

4.1. Output Transformation

170 As mentioned, the system is *over-actuated* in regard to the number of inputs, as the position and the two chamber pressures cannot be controlled individually. Hence, it is desirable to construct an output transformation enabling the possibility to consider more *appropriate* states than the actual pressure states. The following takes offset in the assumption that the effective bulk moduli of the cylinder chambers equal each other, i.e. $\beta_{Ae} = \beta_{Be} = \beta_e$, which is a reasonable assumption if the chamber pressures are sufficiently high (> 20 [bar]).

175 The chosen output states are the piston position, the virtual load pressure P_L that is proportional to the piston output force, and the *level pressure* P_δ which may be considered a weighted sum of the chamber pressures, with the load pressure and level pressure defined by:

$$P_L = P_A - \alpha P_B, \quad P_\delta = P_A + \delta P_B, \quad \delta > 0 \quad (30)$$

Combining P_L, P_δ then P_A, P_B may be expressed as:

$$P_A = \frac{\alpha P_\delta}{\alpha + \delta} + \frac{\delta P_L}{\alpha + \delta}, \quad P_B = \frac{P_\delta}{\alpha + \delta} - \frac{P_L}{\alpha + \delta} \quad (31)$$

The nonlinear load- and level pressure dynamics is obtained as Eqs. (32), (33).

$$\dot{P}_L = \dot{P}_A - \alpha \dot{P}_B \quad (32)$$

$$= \frac{\beta_e}{\rho V_A} (\rho(Q_A - Q_{vA}) + \alpha(Q_B + Q_{vB}) - A_A(a^2 + \rho) \dot{x}_P) \quad (32)$$

$$\dot{P}_\delta = \dot{P}_A + \delta \dot{P}_B + \dot{\delta} P_B \quad (33)$$

$$= \frac{\beta_e}{\rho V_A} (\rho(Q_A - Q_{vA}) - \delta(Q_B + Q_{vB}) - A_A(\rho - \alpha\delta) \dot{x}_P) \quad (33)$$

$$+ \frac{\dot{\delta}}{\delta + \alpha} (P_\delta - P_L)$$

It is notable that δ e.g. has significant impact on the volume flow of Eq. (33), i.e. the piston velocity dependent term. The volume flow may significantly influence on the level pressure, hence the valve flows required to control this and the dynamic couplings. Hence it is found sensible to choose $\delta = \rho/\alpha$, thereby decoupling the volume flow from the level pressure dynamics in Eq. (33),

whereas it introduces another piston velocity dependent term due to $\dot{\delta}$, ρ . The influence of this is analyzed subsequently. Using $\delta = \rho/\alpha$, Eqs. (32), (33) modifies to:

$$\dot{P}_L = \frac{\beta_e}{\rho V_A} (\rho(Q_A - Q_{vA}) + \alpha(Q_B + Q_{vB}) - A_A(\alpha^2 + \rho)\dot{x}_P) \quad (34)$$

$$\dot{P}_\delta = \frac{\beta_e}{\rho V_A} (\rho(Q_A - Q_{vA}) - \delta(Q_B + Q_{vB}) - \dot{x}_P \frac{A_A \rho}{\beta_e} \frac{\delta + 1}{\delta + \alpha} (P_\delta - P_L)) \quad (35)$$

Letting p_L , p_{δ_0} denote the deviation variables of P_L , P_δ , the linear pressure dynamics may be obtained as:

$$\begin{aligned} \dot{p}_{\delta_0} &= \frac{\beta_e}{V_{0A}(\alpha + \delta_0)} \left((\alpha + \delta_0) \left(K_{\Delta\omega} \omega_m - q_{vA} - \frac{q_{vB}}{\alpha} \right) - (K_{\delta p\delta} + K_{\delta p}) p_\delta - (K_{\delta pL} - K_{\delta p}) p_L \right) \\ &\quad - K_{\delta xd} \dot{x}_P - K_{\delta xp} x_P \end{aligned} \quad (36)$$

$$\begin{aligned} \dot{p}_L &= \frac{\beta_e(\alpha + \delta_0)}{V_{0A}\delta_0} \left(\frac{\delta_0}{\alpha + \delta_0} \left(K_{\Delta\omega} \omega_m - q_{vA} + \frac{q_{vB}}{\delta_0} \right) - A_A \dot{x}_P \right. \\ &\quad \left. - \frac{\delta_0 K_{Lp\delta}}{(\alpha + \delta_0)^2} p_\delta - \frac{\delta_0 K_{LpL}}{(\alpha + \delta_0)^2} p_L \right) \end{aligned} \quad (37)$$

$$\begin{aligned} K_{\Delta\omega} &= K_{Aq} - \frac{K_{Bq}}{\alpha}, \quad K_{\delta p\delta} = \alpha K_{Aqp} - \frac{K_{Bqp}}{\alpha} \\ K_{\delta pL} &= \delta_0 K_{Aqp} + \frac{K_{Bqp}}{\alpha}, \quad K_{\Delta\omega} = K_{Aq} + \frac{K_{Bq}}{\delta_0} \\ K_{Lp\delta} &= \alpha K_{Aqp} + \frac{K_{Bqp}}{\delta_0}, \quad K_{LpL} = \delta_0 K_{Aqp} - \frac{K_{Bqp}}{\delta_0} \\ K_{\delta p} &= \frac{\dot{x}_P A_A(\delta_0 + 1)}{\beta_e}, \quad K_{\delta xd} = \left. \frac{\partial \dot{P}_\delta}{\partial \dot{x}_P} \right|_{x_0}, \quad K_{\delta xp} = \left. \frac{\partial \dot{P}_\delta}{\partial x_P} \right|_{x_0} \end{aligned}$$

From the above the output transformation may be established as:

$$\tilde{\mathbf{y}} = \mathbf{W}_2 \mathbf{y}, \quad \tilde{\mathbf{y}} = \begin{bmatrix} x_P \\ p_L \\ p_\delta \end{bmatrix}, \quad \mathbf{W}_2 = \begin{bmatrix} 1 & 0 & 0 \\ 0 & 1 & -\alpha \\ 0 & 1 & \delta_0 \end{bmatrix} \quad (38)$$

4.1.1. Output Transformation Analysis

In order to investigate the consequences of the output transformation, this is evaluated from Eq. (29) with Eq. (38) and the input transformation matrix $\mathbf{W}_1 = \mathbf{I}$. The resulting RGA numbers as a function of frequency are shown in figure 6.

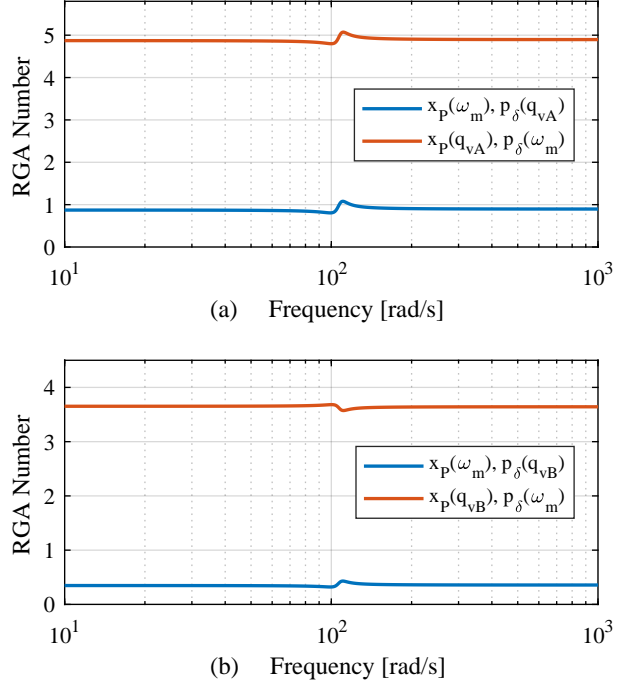


Figure 6: (a) RGA number for $\tilde{\mathbf{G}}_e$ with output transformation (38) utilizing inputs ω_m , q_{vA} . (b) RGA number for $\tilde{\mathbf{G}}_e$ with output transformation (38) utilizing inputs ω_m , q_{vB} .

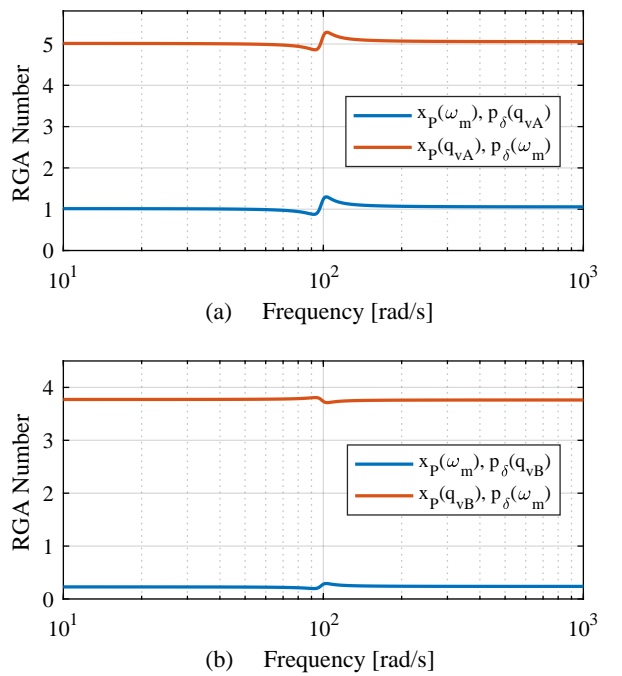


Figure 7: RGA numbers for $\tilde{\mathbf{G}}_e$ with output transformation (38) and volume estimation error of 40 % increase in the B -line. (a) Inputs ω_m and q_{vA} are utilized. (b) Inputs ω_m and q_{vB} are utilized.

185 It is found that the impact of coupled effects of the transformed system is significantly reduced.

190 An additional property to consider is the sensitivity of the output transformation. Exact information on cylinder dimensions are normally available, however, the initial volumes may be difficult to determine dependent on the application. To investigate the sensitivity to an inaccurate initial volume estimate, hence an inaccurate δ_0 , consider figure 7, where V_{B0} is increased by 40 %. It is found that the volume estimation error influences cross 215 couplings to some extend, but still a significant improvement is achieved with the proposed output transformation.

4.2. Input Transformation

Based on the level- and load pressure dynamics Eqs. (36), (37), novel inputs in terms of the *level flow* q_{δ_0} and the *load flow* q_L are defined as Eqs. (39), (40):

$$q_\delta = (\alpha + \delta_0) \left(K_{\Delta_0\omega} \omega_m - q_{vA} - \frac{q_{vB}}{\alpha} \right) \quad (39)$$

$$q_L = \frac{\delta_0}{\alpha + \delta_0} \left(K_{\Lambda\omega} \omega_m - q_{vA} + \frac{q_{vB}}{\delta_0} \right) \quad (40)$$

$$\dot{p}_\delta = \frac{\beta_e}{V_{0A}(\alpha + \delta_0)} \left(q_\delta - (K_{\delta p\delta} + K_{\delta p})p_\delta - (K_{\delta pL} - K_{\delta p})p_L \right) - K_{\delta xd}\dot{x}_P - K_{\delta xp}x_P \quad (41)$$

$$\dot{p}_L = \frac{\beta_e(\alpha + \delta_0)}{V_{0A}\delta_0} \left(q_L - A_A\dot{x}_P - \frac{\delta_0 K_{Lp\delta}}{(\alpha + \delta_0)^2} p_\delta \right) - \frac{\delta_0 K_{LpL}}{(\alpha + \delta_0)^2} p_L \quad (42)$$

The choice of q_{δ_0} and q_L is such that the influence of the shaft velocity and proportional valve flows are *hidden* 200 from the pressure level and load pressure gradients, and contained in these *input flows*. Control structures using these new inputs can thereby be designed independent of the value and sign of the shaft velocity, and of the valve signal allocation. 205

It should be noted that the flow gain K_{Aq} of the combined displacement pump, i.e. pumps A and C, changes 210 value based on the sign of the shaft velocity, as pump C is either providing flow to the actuator ($\omega_m > 0$) or idling its flow through the check valve ($\omega_m < 0$). Hence, the sign of $K_{\Delta_0\omega}$ changes dependent on the sign of ω_m . $K_{\Lambda\omega}$ is on the other hand always positive regardless of the sign of ω_m .

The relation between the original input \mathbf{u} and the transformed input $\tilde{\mathbf{u}}$ is obtained from the inverse input

transformation matrix \mathbf{W}_1^{-1} given by Eq. (43).

$$\tilde{\mathbf{u}} = \mathbf{W}_1^{-1} \mathbf{u}, \quad \tilde{\mathbf{u}} = [q_L \ q_{\delta_0} \ q_0]^T, \quad \mathbf{u} = [\omega_m \ q_{vA} \ q_{vB}]^T$$

$$\mathbf{W}_1^{-1} = \begin{bmatrix} \frac{\delta_0 K_{\Lambda\omega}}{\alpha + \delta_0} & -\frac{\delta_0}{\alpha + \delta_0} & \frac{1}{\alpha + \delta_0} \\ (\alpha + \delta_0) K_{\Delta_0\omega} & -(\alpha + \delta_0) & -\frac{\alpha}{\alpha + \delta_0} \\ v_{31} & v_{32} & v_{33} \end{bmatrix} \quad (43)$$

Here v_{31}, v_{32}, v_{33} are entries that may be chosen arbitrarily. The flow q_0 is a *flow constraint* that may be chosen dependent on the desired distribution of the valve signals. The simplest flow constraint would be $q_0 = 0$, and dependent on the flow constraint, various input transformation matrices may be established.

By evaluation of Eq. (40), it makes sense to construct the input transformation matrix such that the valve flows do not influence the load flow, i.e. such that the piston motion ideally is only driven by ω_m . This may be achieved by choosing parameters $v_{31} = 0$, $v_{32} = 1$, $v_{33} = -1/\delta_0$, and q_0 according to:

$$q_0 = q_{vA} - \frac{q_{vB}}{\delta_0} = 0 \quad (44)$$

The resulting input \mathbf{u} is then given by:

$$\mathbf{u} = \mathbf{W}_1 \tilde{\mathbf{u}} = \begin{bmatrix} \frac{\alpha + \delta_0}{\delta_0 K_{\Lambda\omega}} q_L \\ \frac{K_{\Delta_0\omega} \alpha}{\delta_0 K_{\Lambda\omega}} q_L - \frac{\alpha}{(\alpha + \delta_0)^2} q_{\delta_0} \\ \frac{K_{\Delta_0\omega} \alpha}{K_{\Lambda\omega}} q_L - \frac{\alpha \delta_0}{(\alpha + \delta_0)^2} q_{\delta_0} \end{bmatrix} \quad (45)$$

4.2.1. Input Transformation Analysis

From the fact that $\alpha > 0$, $\delta_0 = \delta_0(\mathbf{x}) > 0$, $K_{\Lambda\omega} > 0$ and Eq. (44) being satisfied, it is found that the sign of q_L is determined by the sign of ω_m .

However, the flows q_{vA}, q_{vB} can only draw flow from the respective transmission lines, i.e. $q_{vA} \geq 0$, $q_{vB} \geq 0$, hence inducing a constraint to the level pressure control. This cannot be accounted for in the input transformation, but must be considered for proper performance. Eq. (43) assumes that the transformed flows are realizable in order to properly distribute the physical control signals, hence the transformed flows must be limited to realizable values prior to evaluation of Eq. (43).

Since the performance of the motion control is considered of higher priority than that of the level pressure control, the load flow q_L should ideally not be influenced, while the achievable level flow q_δ may be constrained. From Eq. (39) the constraint $q_{vA} \geq 0$, $q_{vB} \geq 0$ induces the restriction:

$$0 \leq q_{vA} + \frac{q_{vB}}{\alpha} \Rightarrow q_\delta \leq (\alpha + \delta_0) K_{\Delta_0\omega} \omega_m \quad (46)$$

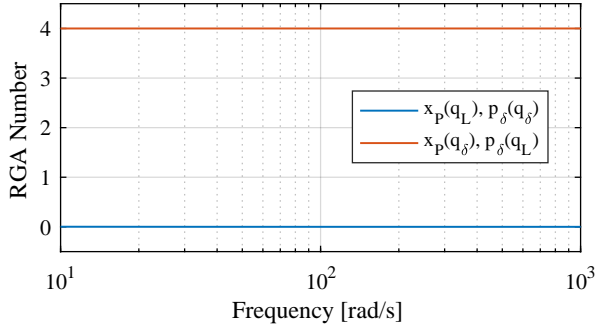


Figure 8: RGA numbers for $\tilde{\mathbf{G}}_e$ with an ideal δ_0 .

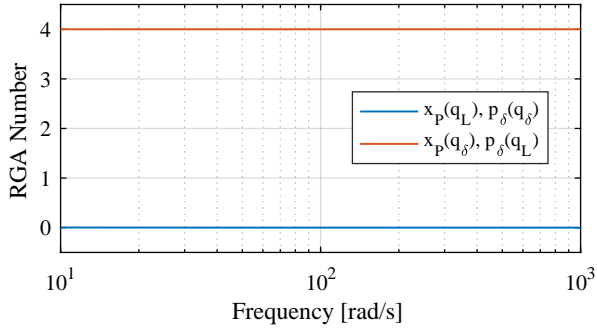


Figure 9: RGA numbers for $\tilde{\mathbf{G}}_e$ with an initial B -line volume estimation error of 40 % increase.

Noting $K_{\Delta\omega}$, a consequence of Eqs. (1), (2) is that $K_{\Delta\omega}$ changes sign according to:

$$K_{\Delta\omega} > 0 \text{ for } \omega_m > 0, \quad K_{\Delta\omega} < 0 \text{ for } \omega_m < 0 \quad (47)$$

From Eq. (47) then Eq. (46) may be formulated as:

$$q_\delta \leq (\alpha + \delta_0)K_{\Delta\omega}\omega_m = (\alpha + \delta_0)|K_{\Delta\omega}|\omega_m \geq 0 \quad (48)$$

Utilizing Eq. (40) while noting Eq. (44), then an upper bound on q_{δ_0} may be established as:

$$q_\delta \leq (\alpha + \delta_0)K_{\Delta\omega}\omega_m = \frac{(\alpha + \delta_0)^2}{\delta_0} \frac{K_{\Delta\omega}}{K_{\Delta\omega}} q_L \quad (49)$$

The RGA numbers for the transformed system $\tilde{\mathbf{G}}_e$ are shown in figure 8 for an ideal estimate of δ_0 , and in figure 9 with an initial volume estimation error. From figure 8, then for an ideal δ_0 -estimate, the proposed input-output transformation method provides a nearly perfect decoupling. Furthermore figure 9 imply a low sensitivity to the considered estimation error in δ_0 .

240 5. Level Pressure Control Design

From Section 4 it is found that decentralized control of the transformed system is reasonable in the frequency

ranges below the actuator bandwidths, i.e. the bandwidths for the electric servo drive and the valves. It is desired to maintain the minimum actual chamber pressure (i.e. the minimum of P_A and P_B) at a low level, while still being high enough to guarantee a sufficiently high oil stiffness. Similar to the approach in Section 4, the principles and considerations are investigated based on the decoupled plant model.

5.1. Level Pressure Reference Generator

The following describes how the measured chamber pressures p_A and p_B are mapped into a level pressure reference $p_{\delta,\text{ref}}$, such that a minimum chamber pressure $\min\{p_A, p_B\} = p_{\text{set}}$ can be achieved.

The chamber pressure to be controlled depends on the load acting on the cylinder, with the theoretical cylinder force directly proportional to the load pressure p_L . If the minimum chamber pressure can be fixed to a specified pressure setting, i.e. $\min\{p_A, p_B\} = p_{\text{set}}$, by utilizing the proportional valves, the chamber pressures can be described directly as functions of the load pressure. As neither of the chamber pressures should decrease below p_{set} in normal operation (when pump leakages exceed the pump leakages), a load pressure related switching condition $p_{L,\text{sw}}$ exists where both chamber pressures are equal to p_{set} . This is given by Eq. (50).

$$p_A = p_B = p_{\text{set}} \Rightarrow p_{L,\text{sw}} = p_{\text{set}}(1 - \alpha) \quad (50)$$

For load pressures above and below the condition $p_{L,\text{sw}}$, the chamber pressures can be written as:

$$p_L \geq p_{L,\text{sw}} \Rightarrow p_A = p_L + \alpha p_{\text{set}}, \quad p_B = p_{\text{set}} \quad (51)$$

$$p_L < p_{L,\text{sw}} \Rightarrow p_A = p_{\text{set}}, \quad p_B = \frac{p_{\text{set}} - p_L}{\alpha} \quad (52)$$

From the definition of p_δ , a level pressure reference may then be obtained as:

$$p_{\delta,\text{ref}} = \begin{cases} p_L + (\delta_0 + \alpha)p_{\text{set}} & \text{for } p_L \geq p_{L,\text{sw}} \\ -\frac{\delta_0}{\alpha}p_L + \frac{\alpha + \delta_0}{\alpha}p_{\text{set}} & \text{for } p_L < p_{L,\text{sw}} \end{cases} \quad (53)$$

Since it may not be apparent from Eq. (53), why the prescribed level pressure reference corresponds to controlling only the minimum chamber pressure, this is emphasized by Eq. (54) with the level pressure control error defined as $e_\delta = p_{\delta,\text{ref}} - p_\delta$.

$$e_\delta = \begin{cases} (\delta_0 + \alpha)(p_{\text{set}} - p_B) & \text{for } p_L \geq p_{L,\text{sw}} \\ \frac{\alpha + \delta_0}{\alpha}(p_{\text{set}} - p_A) & \text{for } p_L < p_{L,\text{sw}} \end{cases} \quad (54)$$

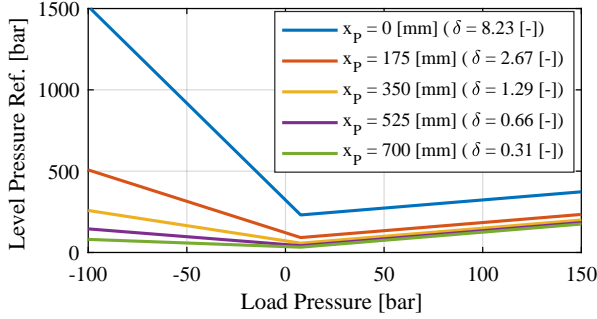


Figure 10: Pressure level reference $p_{\delta_0,\text{ref}}$ as function of load pressure p_L for different piston positions. The pressure setting is $p_{\text{set}} = 25 \text{ [bar]}$ resulting in $p_{L,\text{sw}} \approx 7.7 \text{ [bar]}$.

Finally, it is relevant to consider how the reference $p_{\delta,\text{ref}}$ changes with the load pressure. This is depicted in figure 10 from which it is found that the transition $p_{\delta,\text{ref}}(p_L \geq p_{L,\text{sw}}) \leftrightarrow p_{\delta,\text{ref}}(p_L < p_{L,\text{sw}})$ is bumpless, which is desirable in order to minimize dynamic excitation resulting from level pressure control action.

Due to the definition of p_δ as a weighted sum of the chamber pressures, the reference values do not directly relate to any physical pressures, why the possibly high numerical values of $p_{\delta,\text{ref}}$ is not of concern.

5.2. Level Pressure Control Design

From $p_{\delta,\text{ref}}$, a feasible control law where $C_\delta(s)$ is the compensator, is given by:

$$q_\delta = C_\delta(s)e_\delta = C_\delta(s)(p_{\delta,\text{ref}} - p_\delta) \quad (55)$$

The compensator $C_\delta(s)$ may be designed based on the transfer function q_δ/p_δ from Eq. (41) considering the load pressure-, velocity- and position dependent terms as disturbances. A *simplified* transfer function for this case is given by:

$$\frac{p_\delta(s)}{q_\delta(s)} = \frac{K_{c\delta}}{\tau_\delta s + 1}, \quad K_\delta = \frac{1}{K_{\delta p\delta}}, \quad \tau_\delta = \frac{V_{0A}(\alpha + \delta_0)}{\beta_e K_{\delta p\delta}} \quad (56)$$

The control system is designed based on the piston position resulting in the highest possible time constant τ_{δ_0} , i.e. where the uncompensated phase lag is highest. Utilizing $\delta_0 = \rho_0/\alpha$, $\rho_0 = V_{0B}/V_{0A}$, $V_{0A} = V_A|_{x_0} = V_{A0} + A_A x_{P0}$, $V_{0B} = V_B|_{x_0} = V_{B0} - \alpha A_A x_{P0}$, then τ_δ may be reformulated as Eq. (57), while considering β_e , $K_{\delta p\delta}$ as constants.

$$\tau_\delta = \frac{1}{\beta_e K_{\delta p\delta}} \left(\alpha V_{A0} + \frac{V_{B0}}{\alpha} - (1 - \alpha) A_A x_{P0} \right) \quad (57)$$

The maximum value of τ_δ then corresponds to the minimum possible value of x_{P0} . In figure 11 the frequency

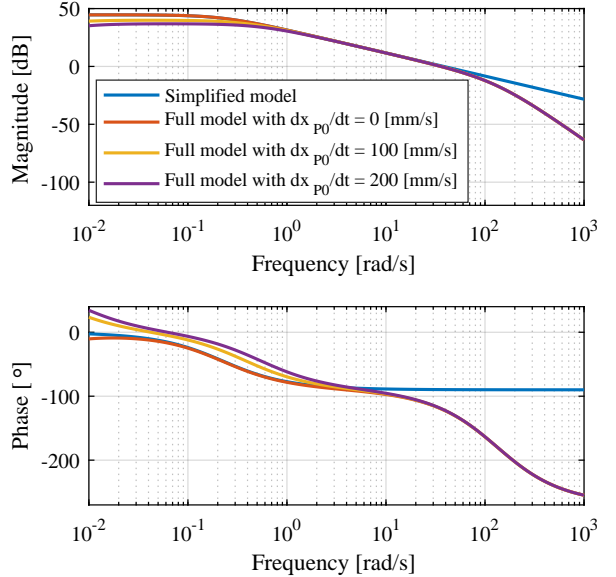


Figure 11: Frequency responses with linearization point: $x_{P0} = x_{P,\text{min}} = -350 \text{ [mm]}$ ($\delta_0 \approx 8.23$), $\dot{x}_{P0} = 100 \text{ [mm/s]}$, $p_A = p_B = p_{\text{set}} = 25 \text{ [bar]}$.

response of Eq. (56) is depicted, when compared to the frequency responses obtained from $\hat{\mathbf{G}}_e$ at different linearization points. It is found that the transfer function (56) conservatively describes the dynamics of p_δ , in the frequency range below the actuator bandwidth.

When selecting the controller for the level pressure control, different considerations should be accounted for. It is desirable to achieve no steady state error in the level pressure to step inputs, why a free integrator is needed in the controller. To counter the introduced phase lag, a zero is included, such that acceptable stability margins can be achieved. To avoid propagation of oscillating pressures into the level pressure control signal, a second order low pass filter is introduced in the controller design, resulting in the controller:

$$C_{\delta_0}(s) = \frac{K_{p\delta_0}s + K_{i\delta_0}}{s} \frac{\omega_f^2}{s^2 + 2\zeta_f\omega_f s + \omega_f^2} \quad (58)$$

The choice of filter frequency is a compromise between attenuating the high frequency content of the level flow reference signal as much as possible, while achieving acceptable stability margins of the closed loop system.

The frequency response of the resulting compensated open loop transfer function is depicted in figure 12 with parameters $\omega_f = 15 \text{ [rad/s]}$, $\zeta_f = 0.6 \text{ [-]}$, $K_{p\delta} = 0.08 \text{ [L/min/bar]}$, $K_{i\delta} = 0.06 \text{ [L/min/bars]}$. With this design procedure, the parametrization of the level pressure control system may be carried out with minimal

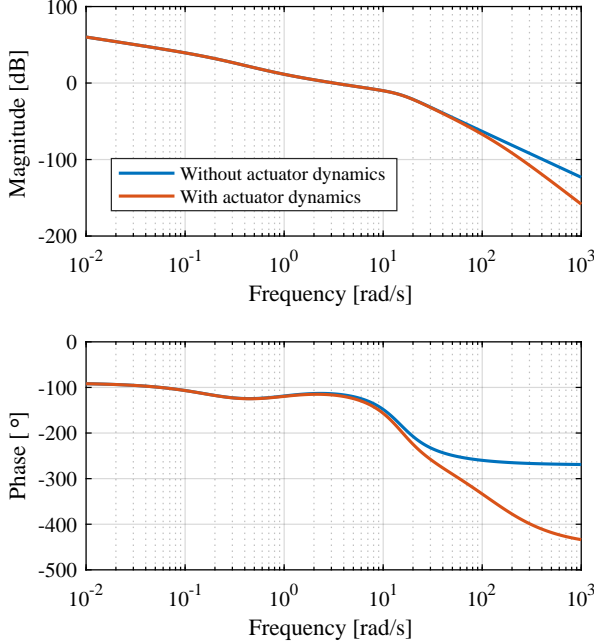


Figure 12: Frequency responses for compensated open loop transfer function with and without actuator dynamics. Linearization point: $x_{P0} = x_{P,min} = -350 ($\delta_0 \approx 8.23$), $\dot{x}_{P0} = 100, $p_A = p_B = p_{set} = 25.$$$

knowledge of the plant parameters, as the simplified model given by Eq. (56) can be used for the control design.

6. Motion Control Design

In order to establish a sufficiently accurate model for design of the motion controller, the consequences of the pressure controller on the motion dynamics is investigated. Combining the level pressure dynamics Eq. (56), the level pressure controller Eq. (58) and the level pressure reference generator Eq. (53), and disregarding the constant p_{set} , then p_δ may be expressed as:

$$p_\delta = H_\delta(s)p_L \quad (59)$$

$$H_\delta(s) = \begin{cases} \frac{\beta_e(C_\delta(s) - K_{\delta pL})}{V_{0A}(\alpha + \delta_0)s + \beta_e(C_\delta(s) + K_{\delta p\delta})}, & p_L \geq p_{L,sw} \\ \frac{-\beta_e(\alpha K_{\delta pL} + C_\delta(s))}{\alpha V_{0A}(\alpha + \delta_0)s + \beta_e(C_\delta(s) + K_{\delta p\delta})}, & p_L < p_{L,sw} \end{cases}$$

Utilizing Eq. (59), the load pressure dynamics Eq. (42) and the force balance Eq. (12), then a transfer function x_P/q_L may be obtained as:

$$\frac{x_P(s)}{q_L(s)} = G_x(s) = \frac{A_A\beta_e(\alpha + \delta_0)^2}{a_2 s^2 + a_1 s + a_0} \frac{1}{s} \quad (60)$$

$$a_2 = \delta_0 M V_{0A}(\alpha + \delta_0)$$

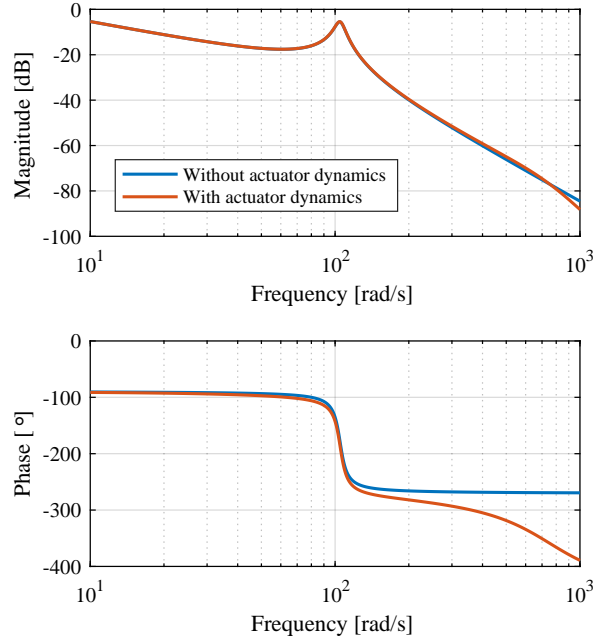


Figure 13: Frequency response for $G_x(s)$ with and without actuator dynamics.

$$a_1 = \beta_e \delta_0 M (H_\delta(s) K_{Lp\delta} + K_{LpL}) + (\alpha + \delta_0) B_v \delta_0 V_{0A}$$

$$a_0 = \beta_e (A_A^2 (\alpha + \delta_0)^2 + B_v \delta_0 (H_\delta(s) K_{Lp\delta} + K_{LpL}))$$

The impact of the filter $H_\delta(s)$ on the pressure dynamics is not immediately clear. However, if this may be neglected, i.e. if the the p_δ -term of the load pressure dynamics Eq. (42) may be neglected, then the motion control design may be conducted while completely disregarding the pressure controller. In that event, the simplified transfer function may be obtained as:

$$\bar{G}_x(s) = \frac{A_A \beta_e (\alpha + \delta_0)^2}{\bar{a}_2 s^2 + \bar{a}_1 s + \bar{a}_0} \frac{1}{s} \quad (61)$$

$$\bar{a}_2 = \delta_0 M V_{0A} (\alpha + \delta_0)$$

$$\bar{a}_1 = \beta_e \delta_0 M K_{LpL} + (\alpha + \delta_0) B_v \delta_0 V_{0A}$$

$$\bar{a}_0 = \beta_e (A_A^2 (\alpha + \delta_0)^2 + B_v \delta_0 K_{LpL})$$

In order to verify whether (61) may be used for control design, the frequency responses of Eqs. (60), (61) depicted in figures 13 and 14 are considered. It is found that closing the level pressure loop only has a slight impact on the motion dynamics, and hence the simplified model (61) is considered applicable for control design.

The linearization point used for parametrization of the motion controller is chosen as the point where the lowest possible natural frequency occur. This may be

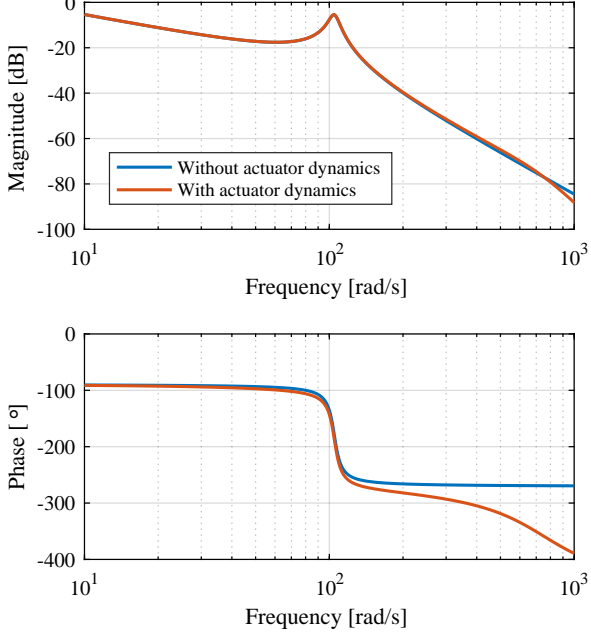


Figure 14: Frequency response for $\tilde{G}_x(s)$ with and without actuator dynamics.

evaluated by the reformulation of $\tilde{G}_x(s)$:

$$\tilde{G}_x(s) = \frac{K_n \omega_n^2}{s^2 + 2\zeta_n \omega_n s + \omega_n^2} \frac{1}{s} \quad (62)$$

$$K_n = \frac{A_A \beta_e (\alpha + \delta_0)^2}{\beta_e (A_A^2 (\alpha + \delta_0)^2 + B_v \delta_0 K_{LpL})}$$

$$\zeta_n = \frac{1}{2} \frac{\sqrt{\delta_0} (B_v V_{0A} (\alpha + \delta_0) + \beta_e K_{LpL} M)}{\sqrt{\beta_e M V_{0A} (\alpha + \delta_0) ((\alpha + \delta_0)^2 A_A^2 + B_v \delta_0 K_{LpL})}}$$

$$\omega_n = \sqrt{\frac{\beta_e (A_A^2 (\alpha + \delta_0)^2 + B_v \delta_0 K_{LpL})}{\delta_0 M V_{0A} (\alpha + \delta_0)}}$$

As K_{LpL} will be numerically small it is reasonable to assume that $\beta_e (A_A^2 (\alpha + \delta_0)^2) \gg B_v \delta_0 K_{LpL}$. Utilizing this and $\delta_0 = \rho_0 / \alpha$, the natural eigenfrequency is estimated as:

$$\omega_n = \sqrt{\frac{\beta_e A_A^2 \eta_n}{M}}, \quad \eta_n = \frac{(\alpha + \delta_0)^2}{\delta_0 V_{0A} (\alpha + \delta_0)} = \frac{\alpha^2 + \rho_0}{V_{0A} \rho_0}$$

For a constant inertia load, the only term varying with the linearization point is η_n . The term η_n may be evaluated at every linearization point from $\eta_n(x_p)$ when replacing $\rho_0 = \rho = \rho(\mathbf{x})$. This is an upward opening parabolic function and will attain its minimum at the condition:

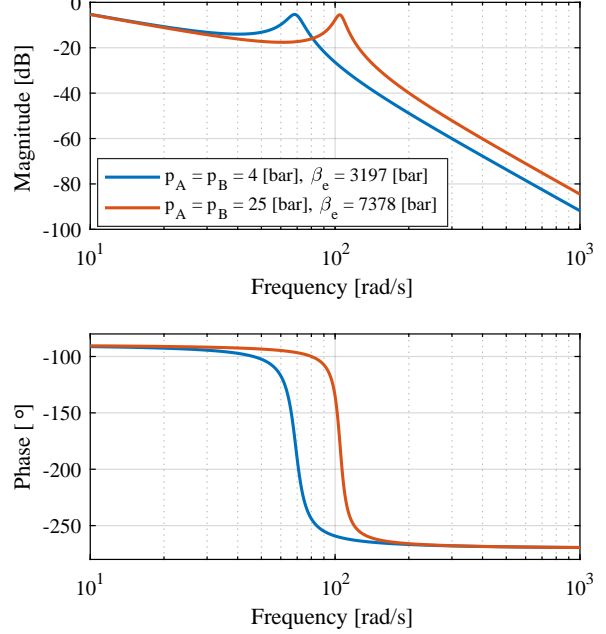


Figure 15: Frequency response for $q_L \rightarrow x_P$ at different pressures.

$$\frac{\partial \eta_n(x_p)}{\partial x_p} = 0 \Rightarrow x_p = \frac{\alpha^2 V_{A0} + V_{B0} - \sqrt{\alpha}(\alpha V_{A0} + V_{B0})}{(1 - \alpha)A_A \alpha}$$

The piston position x_p that satisfies this is thus the position at which the eigenfrequency attains its minimum with respect to x_p , whereby one obtain $\rho = \alpha^{\frac{3}{2}}$, i.e. at the linearization point where $\rho_0 = \alpha^{\frac{3}{2}}$ and $\delta_0 = \sqrt{\alpha}$. Due to the generality of Eq. (62), various compensators may be designed without consideration on how the transformed control signal q_L is distributed between the physical control signals, i.e. the input transformation. Hence a simple PI controller with velocity feed forward is considered for motion control. The frequency response for (62) is depicted in figure 15 for different pressures.

Due to the poor damping of the open loop system, a static load pressure feedback given by Eq. (63) is utilized to realize the open loop frequency response $q_L^* \rightarrow x_p$ depicted in figure 16.

$$q_{L,ref} = q_{L,ref}^* - K_{ad} p_L \quad (63)$$

The value of K_{ad} is chosen to obtain a damping ratio of $\approx 0.5 [-]$.

A PI position controller is designed based on the frequency responses in figure 16.

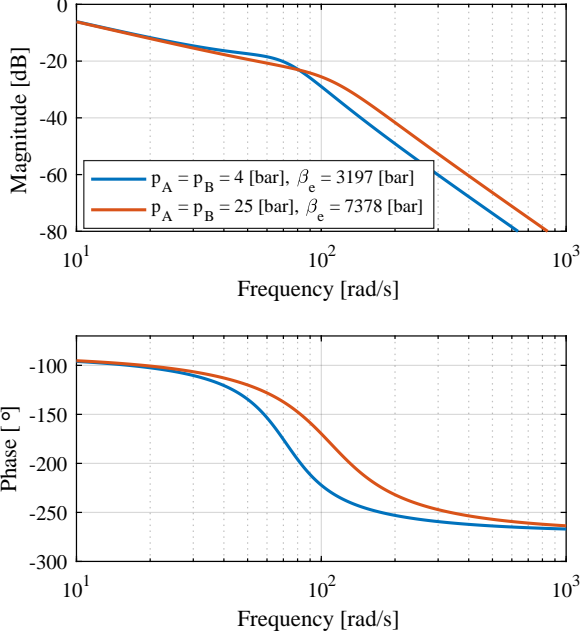


Figure 16: Frequency response for $q_L^* \rightarrow x_P$ at different pressures.

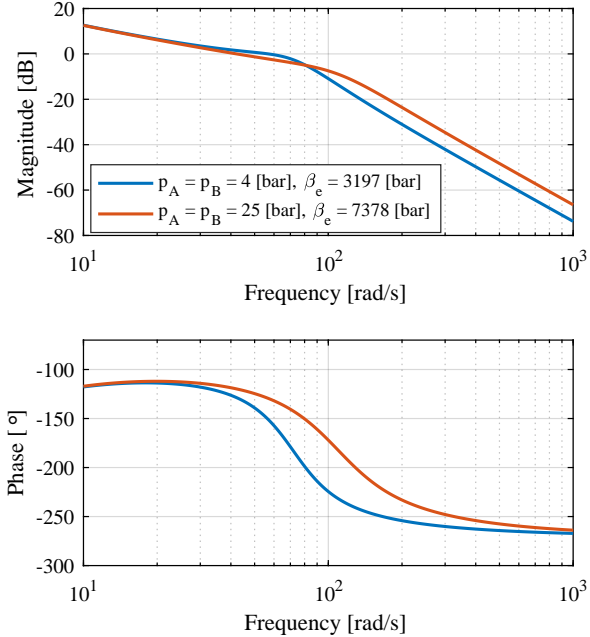


Figure 17: Frequency response of open loop system with motion controller.

Feed forward of the reference velocity is furthermore used to improve the position tracking properties of the closed loop system. With $e_x = x_{P,ref} - x_P$, the final control structure for the motion control system including

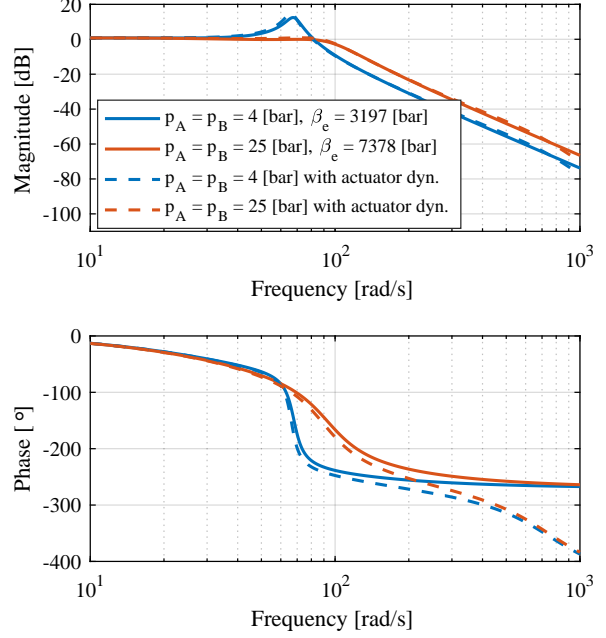


Figure 18: Frequency responses of closed system with motion controller with and without actuator dynamics.

load pressure feedback is thus given by:

$$q_{L,ref}^* = A_A \dot{x}_P + K_p e_x + K_i \bar{e}_x - K_{ad} p_L, \quad \dot{\bar{e}}_x = e_x \quad (64)$$

In (64) the velocity feed forward term is scaled with the piston area to approximately correspond to the static gain of Eq. (62), required to realize the given velocity.

The parameters for the PI motion controller are chosen to yield sufficient stability margins, both for low and high pressure operation. Due to the higher gain and lower bandwidth of the transfer function at low pressures, the low pressure operation poses the most restrictive limitations to the choice of compensator parameters. However, as the pressures will increase during control activity, it is considered reasonable to accept slightly lower stability margins during low pressure operation. As a result, the compensator parameters are chosen as $K_p = 8 [L/min/mm]$ $K_i = 32 [L/min/(mms)]$, such that the following stability margins are realized, here for two specific pressure cases.

$$p_A = p_B = 4 [\text{bar}] : \text{GM} \approx 2.5 [\text{dB}], \text{PM} \approx 30 [\text{°}]$$

$$p_A = p_B = 25 [\text{bar}] : \text{GM} \approx 8.5 [\text{dB}], \text{PM} \approx 60 [\text{°}]$$

The frequency responses of the resulting compensated open loop- and the closed loop transfer functions are shown in figure 17 and 18, respectively, for both high and low pressure operation.

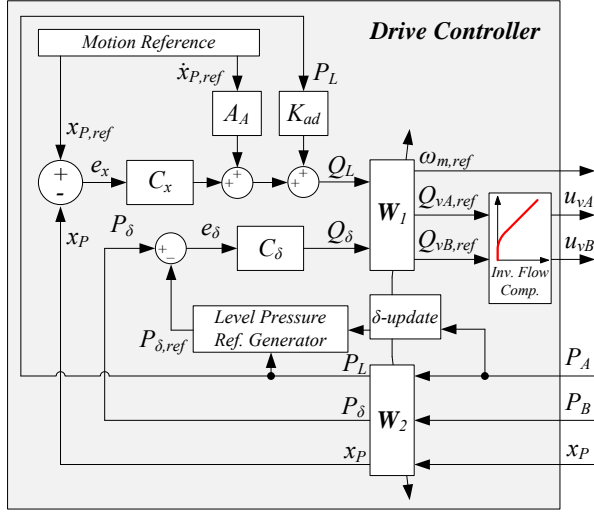


Figure 19: Schematic of complete control system.

7. Experimental Results

The performance of the proposed control structure is evaluated experimentally on the SvSDP prototype drive, with the controller synthesized from the above sections as depicted in figure 19. The objective with the experiments is to validate the proposed control structure for different test cases covering the operating range of the SvSDP drive. Hence, performance is evaluated with external loads in the discrete interval $F_{ext} = [-20 \text{ } -10 \text{ } 0 \text{ } 10 \text{ } 20] \text{ [kN]}$ with a reference trajectory having maximum piston velocities in the discrete interval $|x_{p,ref}|_{max} = [10 \text{ } 50 \text{ } 125 \text{ } 200] \text{ [mm/s]}$, while extracting and retracting the cylinder piston in all cases. Furthermore, in all tests presented the level pressure setting is $P_{set} = 25 \text{ [bar]}$. The results for the different piston reference velocities subjected to different external loads are depicted in figures 20, 21, 22, 23.

From the results it is found that accurate motion tracking is achieved throughout the position reference trajectory, regardless of the external loads applied, and that the position control error is below 500 [\mu m] in almost all cases.

In regard to the pressure control, it is found that the controller strives to maintain the lower chamber pressure at the pressure setting P_{set} whenever this is exceeded. Also, whenever the pump shaft speed is rather low or stationary, the lower chamber pressure tends to the reservoir pressure 1 [bar] (in the plots 0 [bar] due to the relative sensor measurement), which is expected due to the pump leakages. However, the higher chamber pressures remain at the necessary levels to oppose the load forces acting on the cylinder. Also it is found that

$ \dot{x}_{p,ref} _{max} = 200 \text{ [mm/s]}$				
$ \dot{x}_{p,ref} _{max} = 125 \text{ [mm/s]}$				
$ \dot{x}_{p,ref} _{max} = 50 \text{ [mm/s]}$				
$ \dot{x}_{p,ref} _{max} = 10 \text{ [mm/s]}$				
Maximum position control errors in [\mu m]				
$F_{ext} = -20 \text{ [kN]}$	337	624	440	-
$F_{ext} = -10 \text{ [kN]}$	410	248	405	221
$F_{ext} = 0 \text{ [kN]}$	272	156	244	212
$F_{ext} = 10 \text{ [kN]}$	263	176	227	221
$F_{ext} = 20 \text{ [kN]}$	299	134	277	231
RMS position control errors in [\mu m]				
$F_{ext} = -20 \text{ [kN]}$	32	59	55	-
$F_{ext} = -10 \text{ [kN]}$	39	32	44	45
$F_{ext} = 0 \text{ [kN]}$	25	29	38	46
$F_{ext} = 10 \text{ [kN]}$	24	26	39	47
$F_{ext} = 20 \text{ [kN]}$	29	26	40	46
Standard deviation in e_x in [\mu m]				
$F_{ext} = -20 \text{ [kN]}$	29	53	42	-
$F_{ext} = -10 \text{ [kN]}$	36	26	35	30
$F_{ext} = 0 \text{ [kN]}$	22	25	27	31
$F_{ext} = 10 \text{ [kN]}$	20	19	28	31
$F_{ext} = 20 \text{ [kN]}$	25	19	29	29

Table 2: Maximum- and RMS position control errors and standard deviations for all test cases.

when the pump shaft rotary motion is accelerated, and attains even a *small* speed, the lower chamber pressure rapidly builds up and settles in a vicinity of the pressure setting P_{set} , resulting in a proper oil bulk modulus which in turn allow for an efficient position tracking effort. Furthermore it is evident that pressure control performance is not on a level with that of the motion controller. This is mainly ascribed the coupling with the load pressure, the lower valve bandwidth compared to that of the servo drive, and the choice of a conservative pressure control design as a result of this. However, this control objective is secondary, and the performance is indeed acceptable. It may furthermore be observed that the valve signals are active simultaneously as expected from the input transformation, and the constraint (44).

The control performance for all test cases is summarized in table 2 for the maximum- and RMS errors and the error standard deviation, respectively. In general, performance tends to improve from negative external load forces to positive external load forces with maxi-

370 mum speeds in the mid range, whereas performance appear to be less sensitive to this at the lowest and highest speeds. No elaborated explanation on this can be given at this point, but is likely to be due to the leakage characteristics and the exact choice of component sizes. However, in general, the control system provides 375 for satisfactory overall performance, and a high tracking accuracy is achieved in the entire operating range.

8. Conclusion

380 An overall control strategy for a novel over-actuated direct hydraulic drive is proposed and experimentally verified when applied to a prototype of the drive. The proposed control strategy takes offset in an analysis of the dynamic couplings between the states of the drive, which demonstrates strong couplings. An approach to decouple the states through input-output transformations is proposed, resulting in a rather low degree of cross couplings for the transformed system. With the piston position tracking as the primary- and the transmission line pressure levels as the secondary control objectives, state controllers are designed based on the 385 transformed system, taking into account nonlinearities resulting from asymmetric volume variation. Experimental results demonstrate that accurate position tracking control is achieved within the operating range of the drive, while maintaining a satisfactory control performance of the transmission line pressures.

References

- [1] K. Heybrook, J. Larsson, J.-O. Palmberg, Open circuit solution for pump controlled actuators, in: 4th FPNI-PhD Symposium, Sarasota, 2006.
- [2] R. Rahmfeld, M. Ivantsynova, Energy saving hydraulic actuators for mobile machinery, in: 1. Bratislavian fluid power symposium, 1998.
- [3] J. ming Zhenga, S. dun Zhao, , Shu-guoWei, Application of self-tuning fuzzy pid controller for a srm direct drive volume control hydraulic press, Control Engineering Practice 17 (12) (2009) 13981404.
- [4] M. Heikkil, M. Linjama, Displacement control of a mobile crane using a digital hydraulic power management system, Mechatronics 23 (4) (2013) 452 – 461. doi:<http://dx.doi.org/10.1016/j.mechatronics.2013.03.009>.
- [5] N. H. Pedersen, P. Johansen, T. O. Andersen, Lqr feedback control development for wind turbines featuring a digital fluid power transmission system, in: Proceedings of the FPNI Ph.D. Symposium on Fluid Power, 2016.
- [6] J. Komsta, P. Stavrou, Variable speed pump drives for industrial machinery system considerations, Fluid Power Journal.
- [7] B. Brahmer, Cldp - hybrid drive using servo pump in closed loop, in: 8th International Fluid Power Conference Dresden, 2012.
- [8] H. C. Pedersen, L. Schmidt, T. O. Andersen, M. H. Brask, Investigation of new servo drive concept utilizing two fixed displacement units, JFPS International Journal of Fluid Power System 8 (1) (2015) 1–9.
- [9] Z. Quan, L. Quan, J. Zhang, Review of energy efficient direct pump controlled cylinder electro-hydraulic technology, Renewable and Sustainable Energy Reviews 35 (2014) 336346.
- [10] L. Schmidt, D. B. Roemer, H. C. Pedersen, T. O. Andersen, Speed-variable switched differential pump system for direct operation of hydraulic cylinders, in: Proceedings of ASME/Bath 2015 Symposium on Fluid Power & Motion Control, 2015.
- [11] R. Falconi, C. Melchiorri, Dynamic model and control of an over-actuated quadrotor uav, in: Proceedings of the 10th IFAC Symposium on Robot Control, 2012, pp. 192–197.
- [12] J.-E. Moseberg, G. Roppeneker, Feed-forward control of a vehicle with single-wheel actuators, in: Proceedings of the 19th World Congress (IFAC), 2014, pp. 6283–6288.
- [13] C. Knobel, A. Pruckner, T. Buente, Optimized force allocation - a general approach to control and to investigate the motion of over-actuated vehicles, in: IFAC Proceedings Volumes, Vol. 39, 2006, pp. 366–371.
- [14] X. Zhang, V. Cocquempot, Fault tolerant control for an electric 4wd vehicle's path tracking with active fault diagnosis, in: Proceedings of the 19th World Congress (IFAC), 2014, pp. 6728–6734.
- [15] D. Khimani, M. Patil, Fault-tolerant sliding mode control for uncertain over-actuated systems, in: In proceedings of the3rd International Conference on Advances in Control and Optimization of Dynamical Systems, 2014, pp. 748–753.
- [16] T. A. Johansen, T. I. Fossen, Control allocation -asurvey, Automatica 49 (5) (2013) 1087–1103.
- [17] C. S. Kallesøe, R. Wisniewski, T. N. Jensen, A distributed algorithm for energy optimization in hydraulic networks, in: Proceedings of the 19th World Congress (IFAC), 2014, pp. 11926–11931.

Acknowledgments

The authors would like to direct special thanks to Henrik Rahn for his effort in the development of the test bench, simulation models etc. and work with the system in general. Furthermore the authors would like to thank Bosch Rexroth A/S (Denmark) for their support in establishing the SvSDP drive prototype test bench, details on components, efficiency maps and design discussions.

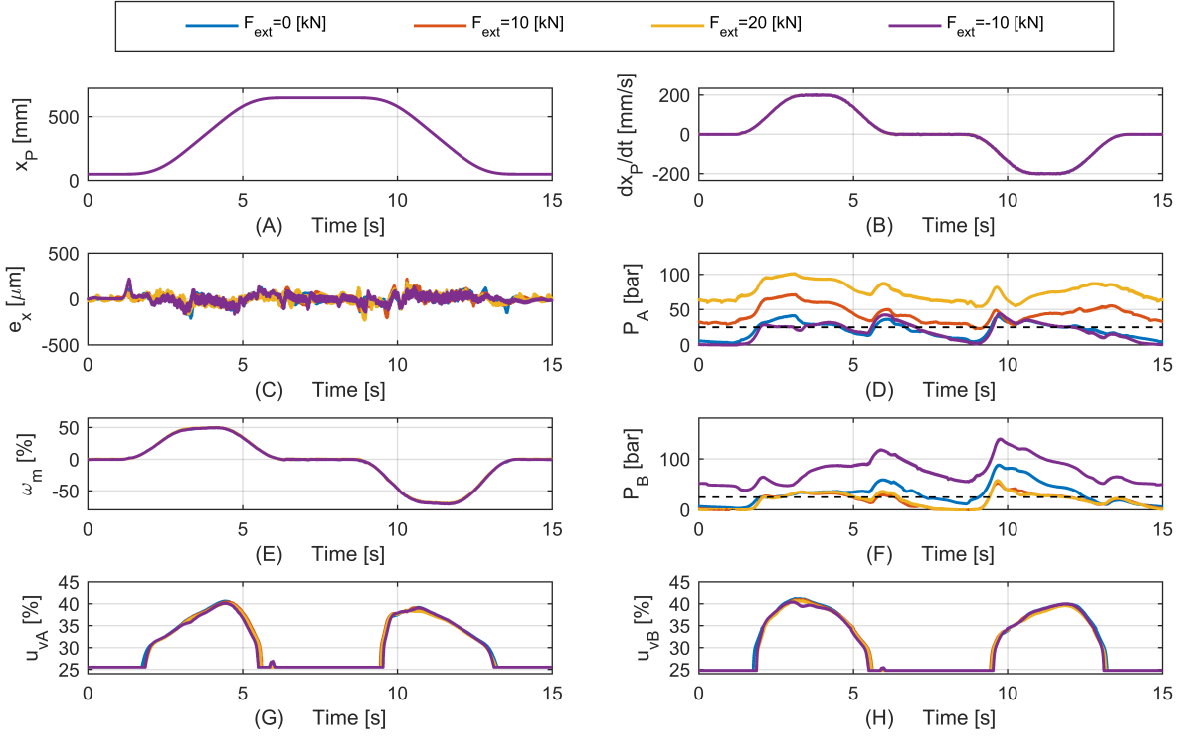


Figure 20: Performance results for SvSDP prototype drive with $|x_{P,ref}|_{max} = 200$ [mm/s] and different F_{ext} . The black line in subplots (D) and (F) indicate the level pressure setting P_{set} .

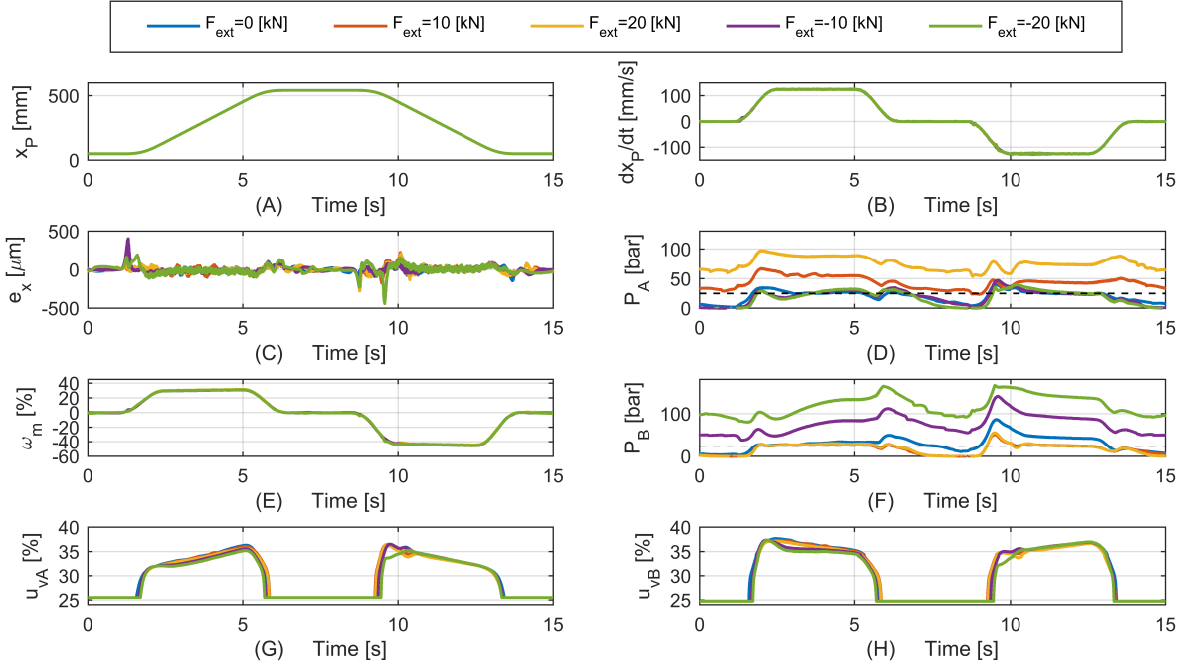


Figure 21: Performance results for SvSDP prototype drive with $|x_{P,ref}|_{max} = 125$ [mm/s] and different F_{ext} . The black line in subplots (D) and (F) indicate the level pressure setting P_{set} .

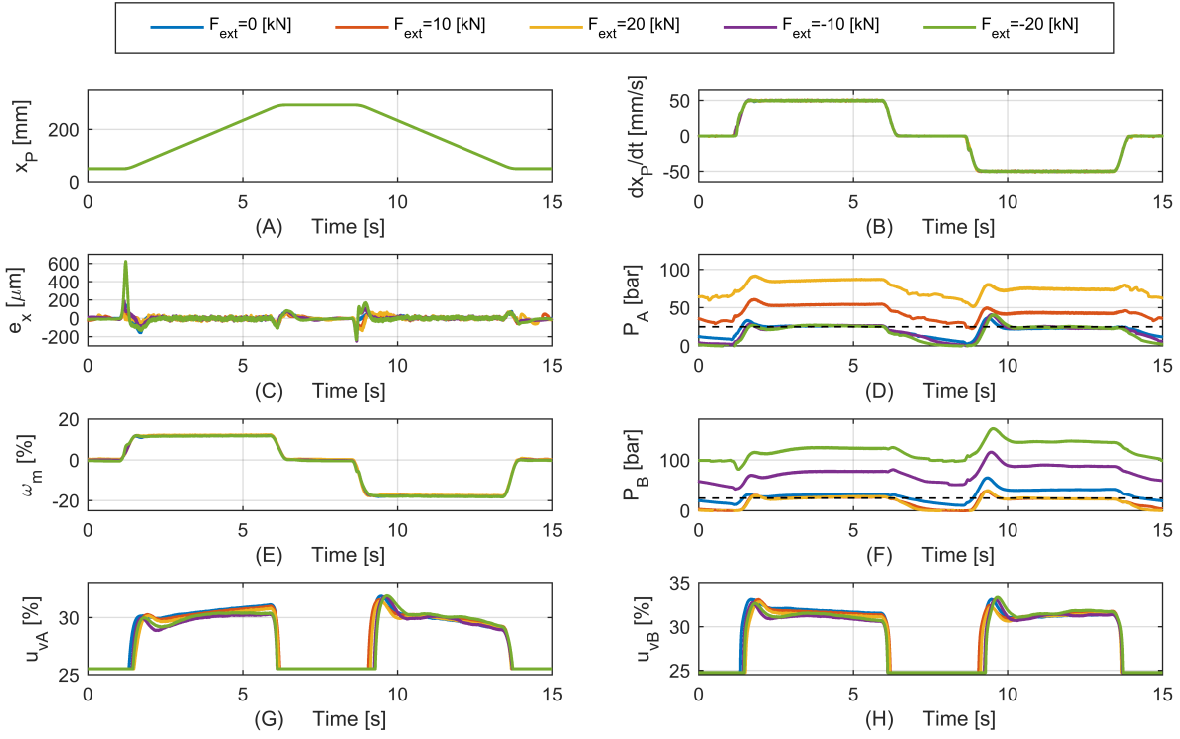


Figure 22: Performance results for SvSDP prototype drive with $|x_{P,\text{ref}}|_{\max} = 50 \text{ [mm/s]}$ and different F_{ext} . The black line in subplots (D) and (F) indicate the level pressure setting P_{set} .

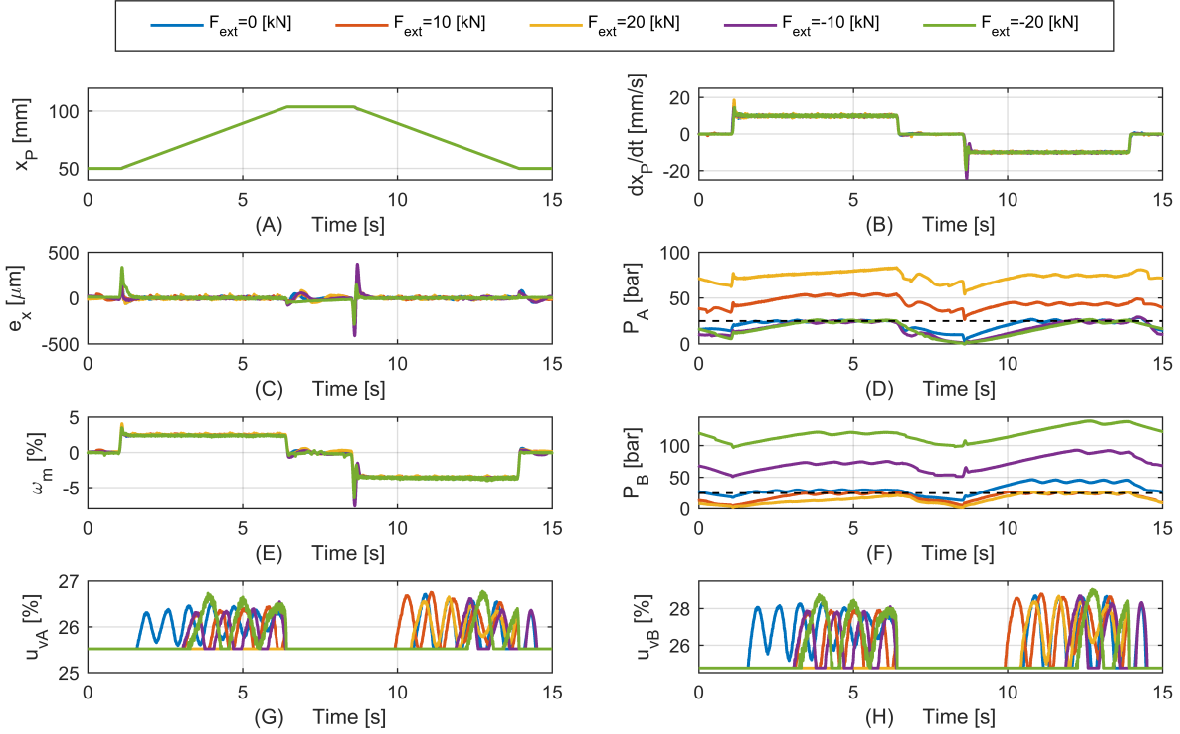


Figure 23: Performance results for SvSDP prototype drive with $|x_{P,\text{ref}}|_{\max} = 10 \text{ [mm/s]}$ and different F_{ext} . The black line in subplots (D) and (F) indicate the level pressure setting P_{set} .